
Category Level 6D Object Pose Estimation from a Single RGB Image using Diffusion

Adam Bethell

University of Adelaide

Ravi Garg

University of Adelaide

Ian Reid

University of Adelaide

Abstract

Estimating the 6D pose and 3D size of an object from an image is a fundamental task in computer vision. Most current approaches are restricted to specific instances with known models or require ground truth depth information or point cloud captures from LIDAR. We tackle the harder problem of pose estimation for category-level objects from a single RGB image. We propose a novel solution that eliminates the need for specific object models or depth information. Our method utilises score-based diffusion models to generate object pose hypotheses to model the distribution of possible poses for the object. Unlike previous methods that rely on costly trained likelihood estimators to remove outliers before pose aggregation using mean pooling, we introduce a simpler approach using Mean Shift to estimate the mode of the distribution as the final pose estimate. Our approach outperforms the current state-of-the-art on the REAL275 dataset by a significant margin.

1 Introduction

Estimating the 6D object pose and 3D object size from an image or video is a vital task that enables a variety of applications in robotics [5, 27] and augmented reality [24, 25]. Historically the vast majority of methods to compute object pose have been instance-based, meaning they require some form of model (often a CAD model) of the particular object of interest. Recently, however, increasing attention has been given to the harder problem of category-level object pose estimation. This task is harder because of the need to handle intra-class variation. The majority of current category-level pose estimation methods require RGB-D or point clouds sensors to provide 3D information as input, which is not available in all situations. Our scenario is the more challenging RGB-based category-level object pose and size estimation in which the pose must be inferred only from a 2D image, and has the additional complication of scale ambiguity.

To address the challenges of category-level pose estimation, previous methods have either: (i) predicted correspondences between the observed object and a Normalised Object Coordinate Space (NOCS) for the object’s category – a kind of generalized PnP; or (ii) regressed the pose via a model learned end-to-end from images and known poses. Although there are many advantages to the latter approach, a significant problem is the multi-hypothesis issue: symmetries, occlusion and scale ambiguity mean there can be multiple feasible poses for a given observation and this causes problems during *training*, since a typical learned model regressed one-to-one from input to output. When multiple hypotheses are equally good the training objective and gradients become unstable, hampering convergence, and degrading the overall inference performance even for non-symmetric objects.

Previous works in instance and category level pose estimation using regression address the issue with specific architectures [4, 15], loss functions [16, 32, 36] and augmenting the ground truth poses [31, 1] but these methods lack generalizability as they are specifically designed for certain objects or require object models. An alternative to a strict one-to-one mapping is to learn a mapping from the input data to a *distribution* over poses. Such a mapping can be captured by a generative diffusion process, and the recent work in [35] (called GenPose) was the first to exploit this, using diffusion to

estimate the pose of a category-level object. Nevertheless, GenPose requires high-quality 3D data (e.g. a lidar point cloud or depth image), fails properly to exploit the fact that the diffusion process is generating a distribution over poses, and employs an expensive and wasteful series of computations to find the mode of the distribution.

Inspired by the idea of using diffusion to model the distribution over pose, in this paper, we introduce a method to find the pose of a category-level object from a single RGB image, and address the apparent wastefulness in the GenPose computations. In particular, we design a score-based diffusion model based on two CNN encoders: one to extract semantic features from the RGB image and the other for geometric features from the predicted relative depth and normals from a large pre-trained model (DMSR [33]). In addition, we also incorporate category-ID data (available from the 2D object detector which is a pre-cursor to any 6D pose estimation) and a global image feature to help set the object scale. These inputs condition a score function that gradually de-noises a set of random pose hypotheses to the correct distribution over pose. If there is a unique pose, this distribution will be “peaky”, close to a delta, but if there are symmetries then the distribution can capture this via multiple modes or uniformity over one or more dimensions

Since the score-based diffusion model stochastically generates a set of hypotheses that represent the distribution over poses, this is ideal for tracking in, for instance, a particle filter framework. But for many applications, we require a single pose estimate. GenPose [35], obtains this estimate by mean pooling. But to robustify this method it first removes outliers by estimating the likelihood of each hypothesis using an entirely separate network (that has the same architecture as the ScoreNet). Low-likelihood samples are removed as outliers prior to taking the mean. Although GenPose shows this improves the performance, it requires an expensive additional calculation; instead, we note that what is required is a maximum likelihood estimate from the distribution, and this can be obtained efficiently and at negligible extra cost via a mode-seeking algorithm such as mean shift [3] improving the inference speed by 15%.

We evaluate our method on the REAL275 dataset and achieve superior performance to existing methods for RGB-based category-level object pose estimation with a 55% increase on the strict 10^o10cm metric and 18% on the IoU75 metric. Our main contributions are summarized as follows:

- We propose the first framework for RGB-based category-level object pose and size estimation that addresses the multi-hypothesis problem by modelling the pose distribution using denoising diffusion models.
- We propose a simpler and more computationally efficient method for estimating the object pose and size from the pose hypotheses sampled using a score-based diffusion model.
- Our method achieves significant improvements over the previous RGB-based category-level object pose estimation methods, setting a new SOTA on the REAL275 benchmark.

2 Related Work

2.1 RGB-D Based Category Level Object Pose Estimation

The task of category-level object pose estimation is to predict the object poses of novel objects from a certain class. Normalised Object Coordinate Space (NOCS) [31] approaches the task by introducing a normalised canonical coordinate space for all objects in a category and uses this space to generate 3D-3D correspondences from which the Umeyama algorithm [28] can estimate the pose. The correspondences are created using Mask-RCNN [8] to detect objects and then a CNN head to predict each dimension of the NOCS coordinates in the image plane. To estimate the NOCS representation of the object the notion of Shape Prior Deformation is introduced by [26] where a category shape prior is used as input to output a deformation field which is used to create an instance shape of the object for alignment with the NOCS coordinates using the depth information.

SGPA [1] extends this idea to transformers to leverage the attention mechanism between the image, depth map and shape prior. The NOCS representation is also used as additional supervision by [32], [16] and [36] while directly regressing the pose from the RGB-D image. As previously mentioned the regression methods inherently suffer from the multi-hypothesis issue so [15] and [4] design symmetry-aware loss functions to address the issue. Similar to the iterative deformation method [32], [2] use an analysis by synthesis style pose estimation method where a VAE and warping operations

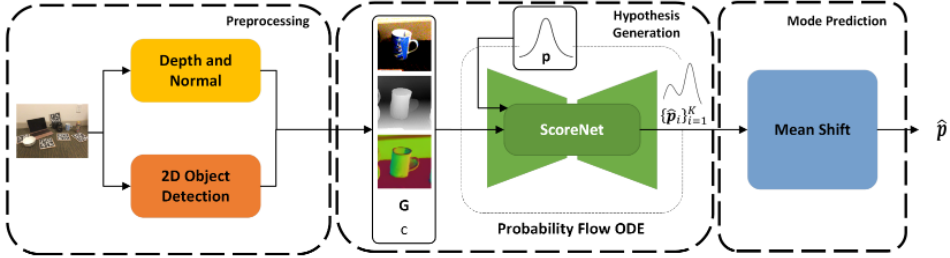


Figure 1: An overview of our method. **Preprocessing:** The input image is passed through a depth and normal predictor and a 2D object detector to get the cropped images, global image feature \mathbf{G} and category ID c . **Hypothesis Generation:** Pose hypotheses are initialised using Gaussian Noise and pass through the Probability Flow ODE and ScoreNet to generate the final pose hypotheses $\hat{\mathbf{p}}_1 \dots \hat{\mathbf{p}}_K$. **Mode Prediction:** Mean Shift is then run on the pose hypotheses to get the final pose estimate $\hat{\mathbf{p}}$.

are used to generate images from a given pose and a segmented image. The perceptual loss between the generated and observed image is minimised by optimising the pose and latent shape code.

2.2 RGB Based Category Level Object Pose Estimation

The analysis by synthesis method presented in [2] is also trained for RGB images and introduces a baseline for RGB-based category-level object pose estimation. While this method produced accurate rotations, there were high translation errors due to scale ambiguity. CPS++ [19] trains a regression network for object pose and size estimation using synthetic data with an additional refinement stage using depth for transferring to real data. The scale ambiguity present in the analysis by synthesis method is addressed in MSOS [13] which utilises two branches: one for the NCOS representation and another for the size prediction by predicting a metric scale object mesh to render a depth map in order to estimate the pose as in the RGB-D NOCS methods. A similar method is introduced in OLD-Net [7] which estimates the object depth and NOCS map using a shape prior and positional features. The most recent RGB method [33] decouples the NOCS predicted and metric scale prediction using the observed image, a shape prior and predicted relative depth and normals from a pre-trained large-scale model as input to a transformer to extract features before two separate networks for 2D-3D correspondences and metric scale recovery. While this method produces SOTA results, their method requires a category shape prior and struggles to address the scale ambiguity causing poor translation accuracy. In contrast to this, we do not require this prior and integrate information from the whole image and an implicitly learned category embedding to address the scale ambiguity.

2.3 Diffusion Models

Score-based generative models have shown impressive capabilities for modelling data distributions by estimating the gradient of the log-likelihood of a sample [10, 22] specifically in a method called Denoising score matching (DSM) [29]. These models have proven particularly powerful and flexible when used in conjunction with conditional inputs and classifier-free guidance. These capabilities have been exploited by GenPose [35] which proposed using conditional score-based models for category-level 6D object pose estimation using point clouds. The score-based model is able to generate multiple pose candidates to address the multi-hypothesis issue before an energy-based model is used to filter the poses before mean pooling to generate a final pose estimate. We use this method as our inspiration but adapt the score model for RGB images rather than point clouds and replace the energy model and mean pooling with Mean Shift for the final pose estimate.

3 Method

In this work our goal is to estimate object pose and size, which is denoted by $\mathbf{p}_i = \{\mathbf{R}_i \in SO(3), \mathbf{t}_i \in \mathcal{R}^3, \mathbf{s}_i \in \mathcal{R}^3\}$. Our system is based on learning a score function to denoise the poses via diffusion. Training this function makes use of dataset D comprising of RGB images, the category of constituent objects and their poses $D = \{(I_i, C_i, \mathbf{p}_i)\}_{i=1}^n$, where $I_i \in \mathbb{R}^{H \times W \times 3}$ represents the training images,

$C_i \in \{1 \cdot L\}$ is the category ID of the objects and \mathbf{p}_i denotes the object's pose. At inference time our goal is to find pose of the object \mathbf{p} given an image I .

As shown in Figure 1, our pose estimation pipeline has three stages: pre-processing, pose hypothesis generation, and mode prediction. Here we outline each of these steps with justification for critical design choices.

3.1 Pre-processing

We extract object bounding boxes, category ID C and global image feature G from the 2D object detector namely MaskRCCN trained on COCO [18] which was finetuned on the target pose estimation dataset by [31]. Additionally, as in [33] we use a pretrained model from Omnidata [6, 12] to extract the relative depths and normals of the object. While [33] opts to estimate the depth and normal from the cropped image of the object using the estimated bounding box, we estimate them from the full image and use Dynamic Zoom In – explained in Appendix A.1.1 to crop them. The dataset D is thus augmented with cropped image I , cropped relative depth I_D , cropped normals I_n , category ID C and global feature G to train the score-based diffusion model called ScoreNet that we describe in next section.

3.2 Pose Hypothesis Generation

It has been well established that pose estimation methods that heavily rely on regression suffer from the multi-hypothesis issue due to object symmetries and occlusions. To address this, we choose to use multiple-pose hypothesis generation by adapting the ScoreNet used in GenPose [35]. In particular, we remove the conditioning on the point cloud that is used in GenPose and instead condition the ScoreNet on RGB image alongside depths, normals, object category, and global image features that are estimated in the pre-processing step.

This results in the following loss for training the diffusion model:

$$L(\theta) = \mathbb{E}_{t \sim \mathcal{U}(\epsilon, 1)} \{ \lambda(t) \mathbb{E}_{\mathbf{p}(0)} \mathbb{E}_{\mathbf{p}(t) | \mathbf{p}(0)} [\| \mathbf{s}_\theta(\mathbf{p}, I_i, I_n, I_D, C, G, t) - \frac{\mathbf{p}(0) - \mathbf{p}(t)}{\sigma(t)^2} \|_2^2] \} \quad (1)$$

where $t \in [0, 1]$ is the continuous time variable used to generate the perturbed pose p sampled using the Variance-Exploding Stochastic Differential Equation (VE-SDE) introduced in [23].

The architecture of our ScoreNet is shown in Figure 5. The network comprises of two CNNs encoding cropped the RGB image of the object I_i and four-channel image consisting of concatenated relative depths and normals respectively. We use sinusoidal positional encoding time which is passed to create time embedding. Category IDs are further encoded to a learned encoding. Output embeddings mentioned above are concatenated with global image feature to form the vector that we condition the denoising diffusion process on. We encode pose via an MLP to a 256-dimensional vector for denoising and use four separate decoder heads to estimate rotation (two heads), scale-invariant translation (SITE) [14] and 3D scale respectively. Further details on these representations can be found in Appendix A.1.2.

Once the ScoreNet has been trained, at inference time the Probability Flow ODE from GenPose [35] can be used with the ScoreNet to sample pose hypotheses $\{\hat{\mathbf{p}}\}_{i=0}^K$.

One can argue that the GenPose [35] can be trivially adapted for pose estimation to use RGB image alone by replacing the ground-truth point cloud (as used in the paper) with back-projected depths predicted using a single view metric depth estimators. We show however that such trivial adaptation grossly under-perform our approach as presented in Table 2.

We believe that this is predominately due to the over-reliance of GenPose on metric scales provided by ground truth point clouds directly. As metric single-view depth estimators – such as [20] that we use for this experiment – are known to produce depths with large scale errors, this simple adaptation of GenPose does not perform well. This justifies the use of relative depths instead of metric in our pipeline. To inform the ScoreNet of the correct scale, we instead opt for a combination of object category-id and global image feature. As most common objects have a limited variation on object scale, informing the pose generator of the object category acts as a strong enough prior for scale estimation. Interestingly DMSR [33] uses an explicit object shape prior to assist in pose estimation

helping scale estimation. However, we believe learning category-specific priors for full object shape is overkill and simple mapping from category ID to scales can suffice. While our category ID embeddings work as the coarse prior for scale, global image feature provides much-needed context and allows for recovery of lost context due to cropping and scaling of objects as well.

3.3 Model Flexibility

In order to make our model more flexible and allow the model to be used with different object detectors and for novel categories without retraining, we take inspiration from classifier-free guidance and drop the conditions during training. Specifically, when a condition is dropped during training it is replaced by a null value \emptyset or a tensor of the same size but filled with zeros. In the case of the category IDs we utilise the zeroth ID as an unknown category.

To further improve the flexibility of the model we follow previous object pose estimation methods and decouple the object detection and pose estimation by generating the image crop for the image, depth and normals using Dynamic Zoom In (DZI) [14, 30]. This process enables the method to work on top of any object detector and increases the robustness to detection errors. Further details can be found in Appendix A.1.1.

3.4 Final Pose Prediction

While the ScoreNet is able to provide pose hypotheses $\{\hat{\mathbf{p}}\}_{i=0}^K$, we need a single pose prediction. In GenPose [35] the final pose estimate $\hat{\mathbf{p}}$ is acquired by filtering the pose hypotheses using an energy model trained to predict the likelihood of each pose for the given point cloud before aggregating the remaining poses using mean pooling. This process requires training another model with the same architecture and using a surrogate for the likelihood during training.

In contrast to this, we do not train another model to predict the likelihood, instead, we propose to return an estimate for the mode of the distribution modelled by the pose hypotheses $\{\hat{\mathbf{p}}\}_{i=0}^K$. We argue that the mode of the distribution should be the final pose estimate rather than the mean pose as given the optimal ScoreNet, the final pose estimate should be the most likely value as opposed to the expected value. Therefore, we utilise the mode-seeking capabilities of Mean Shift [3, 34] to estimate the mean of the distribution from the pose hypotheses. Specifically, we split the pose into its rotation, translation and size components and run Mean Shift++ [11] on each of these to obtain the modes of the distribution before selecting the mode with the highest number of pose hypotheses in its cluster.

3.5 Implementation Details

The predicted relative depth and normals for each image are estimated by the version 2 DPT models pre-trained on Omnidata [6, 12]. We generate the image patches using the results from MaskRCNN [8] as in previous works to enable a fair comparison. Each patch is resized to 256×256 before being fed into the ScoreNet. The CNN encoders are each ResNet-34s [9] with the image encoder’s weights initialised from a pre-trained image classification model trained on ImageNet1K [21]. The final output of the CNN encoders and the global feature from MaskRCNN are 2048 dimensional tensors. The pose encoder is implemented as a 2-layer MLP with hidden dimensions 256 and the time is encoded using the Gaussian Fourier projection from [23] with a single MLP layer. The category embedding has a dimension of 128 and the conditions are dropped randomly at a 10% rate. The rotation, translation and size heads are 3-layer MLPs with hidden dimensions of 512 again with ReLU activation in between all the layers. All experiments were conducted on an NVIDIA RTX 4080 GPU with a batch size of 64 and implemented in PyTorch.

4 Experiments

4.1 Datasets

We conduct our experiments on two benchmark datasets for 6D category-level object pose estimation introduced by NOCS [31]: CAMERA and REAL275. We utilise the convention in NOCS for splitting the training, validation and test sets. The datasets contain 6 categories of common objects: bottle, bowl, camera, can, laptop and mug. The CAMERA dataset contains synthetic images generated

Table 1: Quantitative comparison of RGB-based category-level object pose estimation on the REAL275 dataset.

Method	CAMERA					REAL275				
	IoU50	IoU75	10°	10cm	10°10cm	IoU50	IoU75	10°	10cm	10°10cm
Synthesis	-	-	-	-	-	-	-	14.2	34.0	4.8
MSOS	32.4	5.1	60.8	29.7	19.2	23.4	3.0	29.2	39.5	9.6
OLD-Net	32.1	5.4	74.0	30.1	23.4	25.4	1.9	37.0	38.9	9.8
DMSR	34.6	6.5	81.4	32.3	27.4	28.3	6.1	59.5	37.3	23.6
Ours	22.9	3.2	85.6	22.4	19.2	44.1	6.7	61.3	56.1	32.7
Ours - NG	28.2	4.7	85.6	27.8	23.4	41.3	5.8	67.6	43.9	33.4
Ours - NC	20.0	1.9	85.4	20.9	17.7	33.4	2.7	61.5	51.3	30.6
Ours - NGR	22.9	3.1	85.5	22.1	18.9	45.2	7.2	67.5	56.6	36.6
Ours - S	-	-	98.4	93.4	92.2	-	-	94.5	88.0	83.0

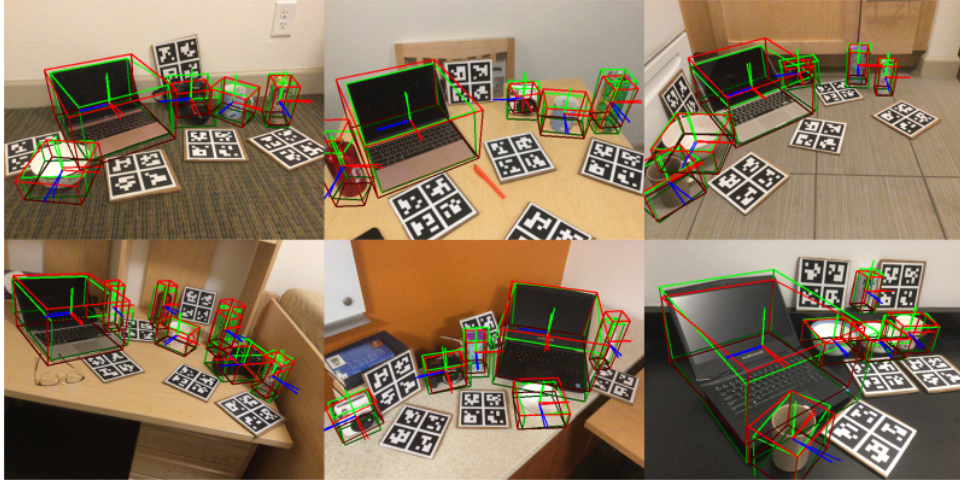


Figure 2: Qualitative results of our method on the REAL275 dataset.

using CAD models of the objects on real background images with 275K training images and 25K test images. The REAL275 dataset contains 3 unique instances of each of the 6 categories in the real world with 7 different scenes each containing a minimum of 5 objects per scene. In total, the REAL275 dataset contains 4300 training images and 2750 testing images.

4.2 Metrics

As in NOCS [31], we adopt mean Average Precision (mAP) in n° and m cm and the 3D Intersection-Over-Union (IoU) at various thresholds as the metrics to evaluate the performance of our object pose and size estimation method. Specifically, we measure the rotation error in degrees and translation error in centimetres where a pose is classed as correct if the rotation error is less than n° and the translation error is below m cm. We utilise $10^\circ 10cm$, 10° and $10cm$ as our thresholds. The 3D IoU is tested for various thresholds namely 50% and 75% and measures the IoU of the ground truth 3D bounding box and the 3D bounding box generated from the estimated pose and size. To handle the symmetries of the bottle, bowl and can, we follow NOCS [31] and ignore the rotation error around the axis of symmetry for the object. Furthermore, the mug follows the symmetrical evaluation when the handle is not visible.

4.3 Comparison with State-of-the-Art

Table 1 shows the quantitative results of our proposed result compared against the existing state-of-the-art (SOTA) for RGB-based category-level object pose estimation on the REAL275 dataset. We report

our results when utilising Mean Shift to generate the final pose estimate from 50 pose hypotheses generated using our ScoreNet (Ours). Furthermore, we report our results when not providing our model with the global feature (Ours - NG) or category IDs (Ours - NC) and only providing the global feature to the translation and size heads (Ours - NGR). Finally, we demonstrate the further potential of the ScoreNet by selecting the closest pose hypothesis to the ground truth (Ours - S).

The results in Table 1 demonstrate the significant performance improvement over the SOTA with a 14% and 52% increase in rotation and translation metrics for the REAL275 dataset. Moreover, we achieve a 55% improvement on the stricter $10^{\circ}10cm$ metric for this dataset. In terms of the 3D IOU metric, our results surpass DMSR with 60% higher IoU50 and 18% improvement on the tighter IoU75 metric. Furthermore, we outperform the rotation on the CAMERA dataset by 5%.

Furthermore, the drop in translation accuracy when dropping the global feature and category ID except in CAMERA for the global feature demonstrates the usefulness of these features for determining the scale of an object. We believe the improved performance in translation without the global feature in CAMERA is due to the synthetic nature of the scene meaning the context provided by this feature is inaccurate.

Figure 2 shows the estimated and ground truth poses for images from the REAL275 dataset. The estimated poses for the symmetric objects generally only differ from the ground truth along the symmetric axis further demonstrating the capability of our method to capture the multiple feasible poses. Furthermore, these images show the significant intra-class variation in the camera class where the poses are accurate for the black cameras but the white cameras have different shapes and semantics which the model is unable to capture.

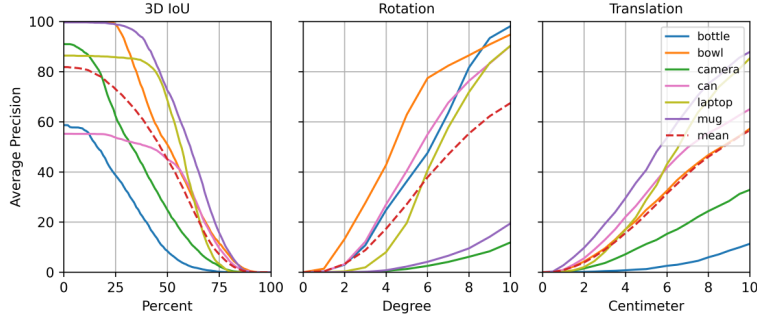


Figure 3: The average precision for various error thresholds for each category.

The average precision of various thresholds for each object class is presented in 3. These results show the dramatic difference in performance for the object classes with the camera and mug performing significantly worse for rotation, due to the large intra-class variation mainly in the lens and the identification of the handle. Furthermore, the bottle and camera struggle in terms of translation possibly because of the large intra-class variation in scales. The high rotation accuracy of the symmetric objects demonstrates the ScoreNet’s ability to generate multiple feasible poses.

Additionally, the results from the ScoreNet when selecting the best pose (Ours - S) and the qualitative results in Figure 4 demonstrate the capability of diffusion models to model the probability distribution of poses accurately. In particular, the rotation distributions of both symmetric and asymmetric objects are captured, highlighted by the tight distribution in Figure 4b and the spread of the hypotheses along the symmetric axis of Figure 4c. Moreover, the distribution of the mug in Figure 4d shows the capability to accurately estimate the final pose without the need for an additional energy model while being more accurate than mean pooling. Further qualitative results of the rotation, translation and size distributions are shown in the Supplementary Material.

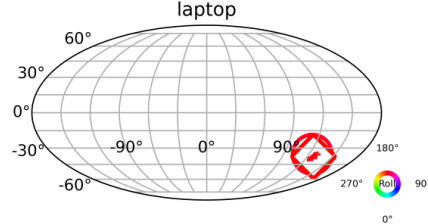
4.4 Ablation Studies

4.4.1 GenPose with Predicted Metric Depth

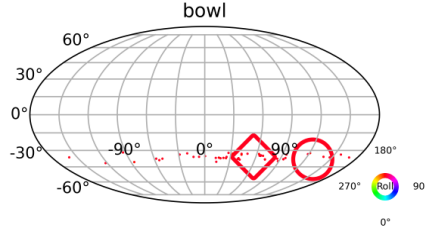
Table 2 illustrates the requirement for our adaptions to the ScoreNet as naively replacing the point cloud in GenPose [35] with the point cloud generated using the estimated metric depth from a SOTA



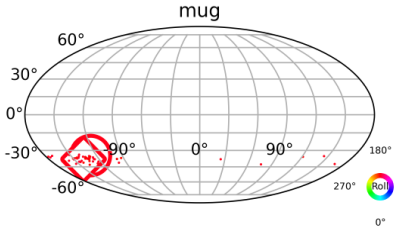
(a) An image from the REAL275 dataset



(b) The distribution of rotations generated for the laptop



(c) The distribution of rotations generated for the bowl



(d) The distribution of rotations generated for the mug

Figure 4: Qualitative results of the predicted rotation distribution for a symmetrical and asymmetrical object. On the left is an example image from the REAL275 dataset. The other images show the rotation distribution with the yaw plotted as the latitude, pitch as the longitude and the roll as the colour. The circle represents the ground truth pose while the diamond shows the final pose estimate with the dots as the individual pose hypotheses.

Table 2: Quantitative comparison of predicted metric depth in GenPose on the REAL275 dataset.

Method	10°	$10cm$	$10^\circ 10cm$
GenPose w/ UniDepth	56.6	26.3	16.0
DMSR	59.5	37.3	23.6
Ours	67.5	56.6	36.6

metric depth estimator UniDepth [20] produces inferior results and even under-performs DMSR [33]. While the rotation prediction is comparable to DMSR the translation is significantly worse due to the large scale errors.

4.4.2 Number of Pose Hypotheses

The results on the $10^\circ 10cm$ metric on the REAL275 dataset are reported in 3 for various numbers of pose hypotheses to explore the number of poses required to accurately model the pose distribution. The largest performance improvement comes from 1 to 10 hypotheses demonstrating the requirement of multiple poses to model the distribution while increasing to 50 has a further increase as the pose distribution is more comprehensively modelled. However, increasing to 100 pose hypotheses does not have any performance gain which can be attributed to pose distribution being sufficiently modelled by 50 hypotheses. Therefore, we chose $K = 50$ as our number of pose hypotheses.

Table 3: Quantitative comparison on the number of pose hypotheses on the REAL275 dataset.

K	IoU50	IoU75	10°	$10cm$	$10^\circ 10cm$
1	38.4	4.9	61.9	50.5	29.2
10	44.0	6.6	66.5	56.0	35.5
50	45.2	7.2	67.5	56.6	36.6
100	44.6	7.1	67.6	56.5	36.5

Table 4: Ablation on the effectiveness of Mean Shift on the REAL275 dataset.

Ranking	Mean Pooling	IoU50	IoU75	10°	$10cm$	$10^\circ 10cm$	FPS
None	✓	45.2	7.1	67.4	56.5	36.4	6.7
Energy	✓	43.6	6.3	68.2	54.1	31.5	3.6
Mean Shift (Ours)	-	45.2	7.2	67.5	56.6	36.6	6.8

Table 5: Results of category-level object pose tracking on REAL275

Method	FPS	$R_{err}(\circ)$	$t_{err}(cm)$
Ours	6.8	9.0	16.8
GenPose	11.6	4.2	1.5

4.4.3 Effectiveness of Mean Shift

The results from the different methods for predicting the final pose estimate from the pose hypotheses are shown in 4. We report the results for three different aggregation and prediction strategies. The baseline method (None) mean pools all the pose candidates to estimate the final pose. The main comparison for our method (Mean Shift) is the "Energy" ranking and mean pooling which is the method used by GenPose for aggregating the pose hypotheses. Our Mean Shift method performs better than the EnergyNet while also being almost twice as fast. However, the mean pooling baseline for our ScoreNet is only marginally worse than the Mean Shift and is just as fast. Therefore, we further demonstrate the potential of Mean Shift using GenPose [35] but replacing the EnergyNet where we achieve a 15% speedup for only 1 % decrease in performance on the $5^\circ 2cm$ metric, the full results are shown in the Supplementary Material.

4.5 Category-level Object Pose Tracking

The iterative nature of the pose hypothesis generation with the ScoreNet enables our method to be easily adapted to category-level pose tracking. The results for our method on the REAL275 dataset are shown in Table 5. Specifically for the first frame, we run pose estimation from pure Gaussian Noise but for all subsequent frames, we start with the pose hypotheses from the previous frame. The details of the algorithm can be found in Appendix B. Our results provide a strong baseline for category-level RGB object pose tracking despite being adapted directly from a single-view prediction method. The major difference between our method and GenPose [35] is the translation error due to the scale ambiguity which could be mitigated by utilising the multiple views during tracking. Furthermore, our method has a lower FPS due to the additional complexity of our ScoreNet.

5 Conclusion

We have proposed an approach for RGB-based category-level object pose estimation using a score-based generative model to generate multiple pose hypotheses. These pose hypotheses model the probability distribution of possible object poses, thus we use Mean Shift to obtain a maximum likelihood estimate from the distribution as our final pose estimate. Our method achieves state-of-the-art performance in category-level object pose estimation for RGB-based methods. Furthermore, we demonstrate the ability of our method to perform object-tracking with minimal adaptions.

As with other diffusion models, the pose hypothesis generation is costly so taking advantage of advances in speeding up diffusion models and actively filtering the poses during the sampling process could improve runtime and performance. Furthermore, our method is reliant on the quality of the predicted depths and normals so future work will focus on minimising this effect. Additional future work involves extending the pose tracking framework to encapsulate the information present across views to help address the scale ambiguity.

References

- [1] Kai Chen and Qi Dou. SGPA: Structure-guided prior adaptation for category-level 6d object pose estimation. In *2021 IEEE/CVF International Conference on Computer Vision (ICCV)*, pages 2753–2762. ISSN: 2380-7504.
- [2] Xu Chen, Zijian Dong, Jie Song, Andreas Geiger, and Otmar Hilliges. Category level object pose estimation via neural analysis-by-synthesis. In Andrea Vedaldi, Horst Bischof, Thomas Brox, and Jan-Michael Frahm, editors, *Computer Vision – ECCV 2020*, Lecture Notes in Computer Science, pages 139–156. Springer International Publishing.
- [3] D. Comaniciu and P. Meer. Mean shift: a robust approach toward feature space analysis. *24(5):603–619*.
- [4] Yan Di, Ruida Zhang, Zhiqiang Lou, Fabian Manhardt, Xiangyang Ji, Nassir Navab, and Federico Tombari. GPV-pose: Category-level object pose estimation via geometry-guided point-wise voting. In *2022 IEEE/CVF Conference on Computer Vision and Pattern Recognition (CVPR)*, pages 6771–6781. IEEE.
- [5] Guoguang Du, Kai Wang, Shiguo Lian, and Kaiyong Zhao. Vision-based robotic grasping from object localization, object pose estimation to grasp estimation for parallel grippers: a review. *54(3):1677–1734*. Number: 3.
- [6] Ainaz Eftekhar, Alexander Sax, Jitendra Malik, and Amir Zamir. Omnidata: A scalable pipeline for making multi-task mid-level vision datasets from 3d scans. In *2021 IEEE/CVF International Conference on Computer Vision (ICCV)*, pages 10766–10776. IEEE.
- [7] Zhaoxin Fan, Zhenbo Song, Jian Xu, Zhicheng Wang, Kejian Wu, Hongyan Liu, and Jun He. Object level depth reconstruction for category level 6d object pose estimation from monocular RGB image. In Shai Avidan, Gabriel Brostow, Moustapha Cissé, Giovanni Maria Farinella, and Tal Hassner, editors, *Computer Vision – ECCV 2022*, Lecture Notes in Computer Science, pages 220–236. Springer Nature Switzerland.
- [8] Kaiming He, Georgia Gkioxari, Piotr Dollar, and Ross Girshick. Mask r-CNN. *pages 2961–2969*.
- [9] Kaiming He, Xiangyu Zhang, Shaoqing Ren, and Jian Sun. Deep residual learning for image recognition.
- [10] Aapo Hyvärinen. Estimation of non-normalized statistical models by score matching.
- [11] Jennifer Jang and Heinrich Jiang. MeanShift++: Extremely fast mode-seeking with applications to segmentation and object tracking. In *2021 IEEE/CVF Conference on Computer Vision and Pattern Recognition (CVPR)*, pages 4100–4111. IEEE.
- [12] Oguzhan Fatih Kar, Teresa Yeo, Andrei Atanov, and Amir Zamir. 3d common corruptions and data augmentation.
- [13] Taeyeop Lee, Byeong-Uk Lee, Myungchul Kim, and In So Kweon. Category-level metric scale object shape and pose estimation. *6(4):8575–8582*. Number: 4.
- [14] Zhigang Li, Gu Wang, and Xiangyang Ji. CDPN: Coordinates-based disentangled pose network for real-time RGB-based 6-DoF object pose estimation. In *2019 IEEE/CVF International Conference on Computer Vision (ICCV)*, pages 7677–7686. IEEE.
- [15] Haitao Lin, Zichang Liu, Chilam Cheang, Yanwei Fu, Guodong Guo, and Xiangyang Xue. SAR-net: Shape alignment and recovery network for category-level 6d object pose and size estimation. In *2022 IEEE/CVF Conference on Computer Vision and Pattern Recognition (CVPR)*, pages 6697–6707. IEEE.
- [16] Jiehong Lin, Zewei Wei, Changxing Ding, and Kui Jia. Category-level 6d object pose and size estimation using self-supervised deep prior deformation networks. In Shai Avidan, Gabriel Brostow, Moustapha Cissé, Giovanni Maria Farinella, and Tal Hassner, editors, *Computer Vision – ECCV 2022*, Lecture Notes in Computer Science, pages 19–34. Springer Nature Switzerland.

[17] Jiehong Lin, Zewei Wei, Yabin Zhang, and Kui Jia. VI-net: Boosting category-level 6d object pose estimation via learning decoupled rotations on the spherical representations. pages 14001–14011.

[18] Tsung-Yi Lin, Michael Maire, Serge Belongie, Lubomir Bourdev, Ross Girshick, James Hays, Pietro Perona, Deva Ramanan, C. Lawrence Zitnick, and Piotr Dollár. Microsoft COCO: Common objects in context.

[19] Fabian Manhardt, Gu Wang, Benjamin Busam, Manuel Nickel, Sven Meier, Luca Minciullo, Xiangyang Ji, and Nassir Navab. CPS++: Improving class-level 6d pose and shape estimation from monocular images with self-supervised learning.

[20] Luigi Piccinelli, Yung-Hsu Yang, Christos Sakaridis, Mattia Segu, Siyuan Li, Luc Van Gool, and Fisher Yu. UniDepth: Universal monocular metric depth estimation.

[21] Olga Russakovsky, Jia Deng, Hao Su, Jonathan Krause, Sanjeev Satheesh, Sean Ma, Zhiheng Huang, Andrej Karpathy, Aditya Khosla, Michael Bernstein, Alexander C. Berg, and Li Fei-Fei. ImageNet large scale visual recognition challenge.

[22] Yang Song and Stefano Ermon. Generative modeling by estimating gradients of the data distribution. In *Advances in Neural Information Processing Systems*, volume 32. Curran Associates, Inc.

[23] Yang Song, Jascha Sohl-Dickstein, Diederik P Kingma, Abhishek Kumar, Stefano Ermon, and Ben Poole. SCORE-BASED GENERATIVE MODELING THROUGH STOCHASTIC DIFFERENTIAL EQUATIONS.

[24] David Joseph Tan, Nassir Navab, and Federico Tombari. 6d object pose estimation with depth images: A seamless approach for robotic interaction and augmented reality. Issue: arXiv:1709.01459.

[25] Fulin Tang, Yihong Wu, Xiaohui Hou, and Haibin Ling. 3d mapping and 6d pose computation for real time augmented reality on cylindrical objects. 30(9):2887–2899. Number: 9 Conference Name: IEEE Transactions on Circuits and Systems for Video Technology.

[26] Meng Tian, Marcelo H. Ang, and Gim Hee Lee. Shape prior deformation for categorical 6d object pose and size estimation. In Andrea Vedaldi, Horst Bischof, Thomas Brox, and Jan-Michael Frahm, editors, *Computer Vision – ECCV 2020*, volume 12366, pages 530–546. Springer International Publishing. Series Title: Lecture Notes in Computer Science.

[27] Jonathan Tremblay, Thang To, Balakumar Sundaralingam, Yu Xiang, Dieter Fox, and Stan Birchfield. Deep object pose estimation for semantic robotic grasping of household objects. Issue: arXiv:1809.10790.

[28] S. Umeyama. Least-squares estimation of transformation parameters between two point patterns. 13(4):376–380. Number: 4 Conference Name: IEEE Transactions on Pattern Analysis and Machine Intelligence.

[29] Pascal Vincent. A connection between score matching and denoising autoencoders. 23(7):1661–1674. Number: 7 Conference Name: Neural Computation.

[30] Gu Wang, Fabian Manhardt, Federico Tombari, and Xiangyang Ji. GDR-net: Geometry-guided direct regression network for monocular 6d object pose estimation. In *2021 IEEE/CVF Conference on Computer Vision and Pattern Recognition (CVPR)*, pages 16606–16616. IEEE.

[31] He Wang, Srinath Sridhar, Jingwei Huang, Julien Valentin, Shuran Song, and Leonidas J. Guibas. Normalized object coordinate space for category-level 6d object pose and size estimation. In *2019 IEEE/CVF Conference on Computer Vision and Pattern Recognition (CVPR)*, pages 2637–2646. IEEE.

[32] Jiaze Wang, Kai Chen, and Qi Dou. Category-level 6d object pose estimation via cascaded relation and recurrent reconstruction networks. In *2021 IEEE/RSJ International Conference on Intelligent Robots and Systems (IROS)*, pages 4807–4814. ISSN: 2153-0866.

- [33] Jiaxin Wei, Xibin Song, Weizhe Liu, Laurent Kneip, Hongdong Li, and Pan Ji. RGB-based category-level object pose estimation via decoupled metric scale recovery.
- [34] Yizong Cheng. Mean shift, mode seeking, and clustering. 17(8):790–799.
- [35] Jiyao Zhang, Mingdong Wu, and Hao Dong. GenPose: Generative category-level object pose estimation via diffusion models.
- [36] Ruida Zhang, Yan Di, Fabian Manhardt, Federico Tombari, and Xiangyang Ji. SSP-pose: Symmetry-aware shape prior deformation for direct category-level object pose estimation. In *2022 IEEE/RSJ International Conference on Intelligent Robots and Systems (IROS)*, pages 7452–7459. ISSN: 2153-0866.
- [37] Yi Zhou, Connelly Barnes, Jingwan Lu, Jimei Yang, and Hao Li. On the continuity of rotation representations in neural networks. In *2019 IEEE/CVF Conference on Computer Vision and Pattern Recognition (CVPR)*, pages 5738–5746. IEEE.

A Architecture and Additional Implementation Details

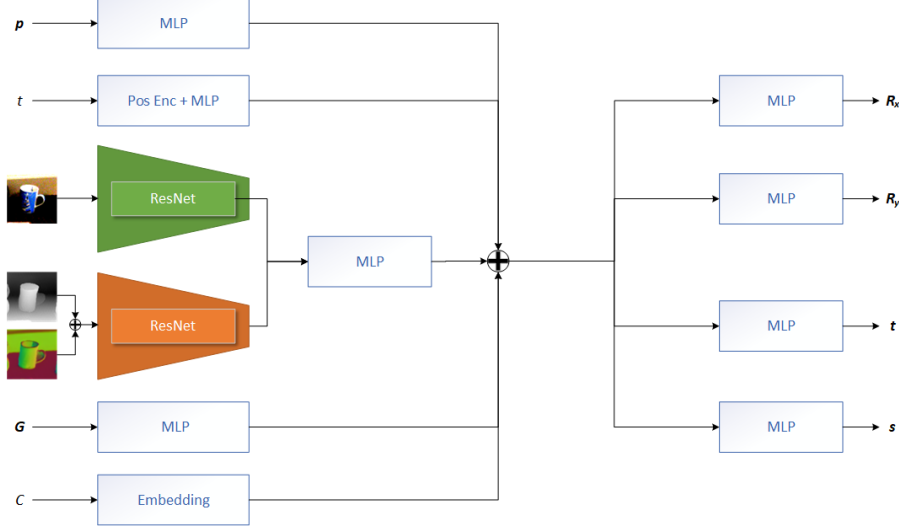


Figure 5: The architecture of our ScoreNet.

A.1 Architecture

A.1.1 Dynamic Zoom In

The input to our CNN encoders are cropped images of the object so following previous object pose estimation methods, we decouple the object detection and pose estimation by generating the image crop for the image, depth and normals using Dynamic Zoom In (DZI) [14, 30]. This process enables the method to work on top of any object detector and increases the robustness to detection errors. Specifically when given an image with ground truth object bounding box centre, (O_x, O_y) , and size, $s = \max(h, w)$, where h and w are the height and width of the bounding box in pixels, we shift (O_x, O_y) uniformly by a ratio of 25% and scale the s by the same ratio. A zoom-in ratio of 1.5 is then used to maintain the aspect ratio and ensure the area containing the object is approximately half the cropped image. At inference time, the detected bounding box is zoomed in with the same ratio (1.5) as in training with no additional shifting or scaling.

A.1.2 Pose Parameterisation

In terms of the pose parameterisation, we parameterise the pose, \mathbf{p} , using a 12D vector with 6D rotation, 3D translation and 3D size components, $\mathbf{p} = [\mathbf{R}|\mathbf{T}|\mathbf{s}]$, $\mathbf{R} \in \mathbb{R}^6$, $\mathbf{T} \in \mathbb{R}^3$ and $\mathbf{s} \in \mathbb{R}^3$. Specifically, the rotation is the continuous 6D representation $[\mathbf{R}_x|\mathbf{R}_y]$ following [37, 30] due to the discontinuity of Euler angles and quaternions. The 6D representation of the rotation can be converted to $SO(3)$ using the following equations:

$$g([\mathbf{a}_1|\mathbf{a}_2]) = [\mathbf{b}_1|\mathbf{b}_2|\mathbf{b}_3] \quad (2)$$

$$\begin{cases} \mathbf{b}_1 = N(\mathbf{a}_1) \\ \mathbf{b}_2 = N(\mathbf{a}_2 - (\mathbf{b}_1 \cdot \mathbf{a}_2)\mathbf{b}_1) \\ \mathbf{b}_3 = \mathbf{b}_1 \times \mathbf{b}_2 \end{cases} \quad (3)$$

Where $N(\cdot)$ is the normalisation function.

The mapping from $SO(3)$ to the 6D representation is defined as:

$$f([\mathbf{a}_1|\mathbf{a}_2|\mathbf{a}_3]) = [\mathbf{a}_1|\mathbf{a}_2] \quad (4)$$

As with other works in RGB-based object pose estimation with cropped images we utilise the Scale Invariant Translation Estimation (SITE) as the translation parameterisation rather than directly predicting $\mathbf{T} = [T_x, T_y, T_z]$. In this parameterization, the translation is represented by $(\delta_x, \delta_y, t_z)$ where δ_x and δ_y represent the offset between the crop centre to the object centre and t_z is the zoomed-in depth. These can be calculated from the bounding box information and the ground truth object centre using Equation 5. The relative offset between the crop and object centres is utilised as this is constant with respect to the Dynamic Zoom In. The translation can be solved using the global information of the image patch, the predicted offset and the zoomed-in depth using Equation 6.

$$\begin{cases} \delta_x = \frac{O_x - C_x}{w} \\ \delta_y = \frac{O_y - C_y}{h} \\ t_z = \frac{T_z}{r} \end{cases} \quad (5)$$

$$\begin{cases} T_x = (\delta_x \cdot w + C_x) \cdot \frac{T_z}{f_x} \\ T_y = (\delta_y \cdot h + C_y) \cdot \frac{T_z}{f_y} \\ T_z = r \cdot t_z \end{cases} \quad (6)$$

where (O_x, O_y) and (C_x, C_y) is the projection of the object centre and centre of the cropped image in the original image, (h, w) is the size of the bounding box in the original image and $r = s_{zoom}/s_o$, s_{zoom} is the size of the resize image patch and $s_o = \max(h, w)$.

The 3D size of the object $\mathbf{s} \in \mathbb{R}^3$ is predicted directly as in VI-Net [17].

B Object Pose Tracking Details

Due to the iterative nature of our pose estimation method, it is able to be used in a pose-tracking framework by utilising the pose hypotheses from the previous frame as the initialisation of the current frame. The full algorithm is outlined below:

Algorithm 1 Pose Tracking Framework

Require: ScoreNet s_θ , initial ground truth pose \mathbf{p}_0 and tracking horizon T .

for $t=1$ **to** T **do**

 Receive current observation I_t
 $\mathbf{z}_1, \mathbf{z}_2, \dots, \mathbf{z}_K \sim \mathcal{N}(\mathbf{p}_{t-1}^K, 0.1^2 I)$ ▷ Add noise to previous pose hypotheses
 $\text{Sample new pose hypotheses } \hat{\mathbf{p}}_{i=1}^K \text{ from } \mathbf{z}_{1:i=1}^K$
 $\text{Estimate current pose } \hat{\mathbf{p}}_t \text{ using Mean Shift}$

end for
